

Radio Properties of Pinwheel Nebulae

J. D. Monnier¹, L. J. Greenhill¹, P. G. Tuthill² and W. C. Danchi³

jmonnier@cfa.harvard.edu, lincoln@cfa.harvard.edu, gekko@physics.usyd.edu.au,
wcd@iri1.gsfc.nasa.gov

ABSTRACT

A small number of dusty Wolf-Rayet stars have been resolved into pinwheel nebulae, defined by their “rotating” spiral dust shells observed in the infrared. This morphology is naturally explained by dust formation associated with colliding winds in a binary system. In order to confirm and further explore this hypothesis, we have observed the known pinwheel nebulae (WR 104 and WR 98a) as well as the suspected binary WR 112 at multiple radio wavelengths with the Very Large Array to search for non-thermal radio emission from colliding winds. The spectrum of each target is nearly flat between 5 and 22 GHz, consistent with the presence of non-thermal emission that is reduced at low frequencies by free-free absorption. This emission must lie outside the radio “photosphere,” leading us to estimate a lower limit to the physical size of the non-thermal emitting region that is larger than expected from current theory. Based on a radio and infrared comparison to WR 104 & 98a, we conclude that WR 112 is a likely candidate pinwheel nebula, but its temporal variability indicates an eccentric binary orbit or a pinwheel viewed nearly edge-on. A sensitive radio survey of IR-bright WRs would stringently test the hypothesis that colliding winds lie at the heart of *all* dusty WR systems. We also discuss the effects of dust obscuration in the ultra-violet and how radio-determined mass-loss rates of pinwheel nebulae (and dusty WR stars in general) may be underestimated due to shadowing effects.

Subject headings: binaries (including multiple): close, stars: Wolf-Rayet, radio continuum: stars, stars: circumstellar matter, stars: winds

¹Harvard-Smithsonian Center for Astrophysics, MS#42, 60 Garden Street, Cambridge, MA, 02138

²School of Physics, University of Sydney, NSW 2006, Australia

³NASA Goddard Space Flight Center, Infrared Astrophysics, Code 685, Greenbelt, MD 20771

1. Introduction

The vast majority of late-WC (carbon-rich) Wolf-Rayet (WR) stars are surrounded by dust shells (Williams et al. 1987a) that absorb stellar flux and re-emit the energy in the infrared (IR). Recently, the geometry of the IR-brightest dust shells have been resolved into spiral plumes that rotate with a ~ 1 yr period: the pinwheel nebulae (Tuthill et al. 1999; Monnier et al. 1999). This morphology has been explained as a consequence of colliding winds with unequal momenta, where dust forms at the interface or in the wake of the winds and is subsequently carried out in the flow (Usov 1991). Because of orbital motion, the direction of the dust flow rotates, generating the observed spiral pattern although the dust motion itself is purely radial. By analyzing the time-dependent morphology, important orbital and wind parameters, such as the period, inclination angle, eccentricity, and even the distance (when combined with observed terminal wind speeds), can be determined with high precision (Monnier 1999; Tuthill et al. 2001).

These observations have led to a more unified picture of the dusty Wolf-Rayet stars in terms of interacting wind (binary) systems. Williams & van der Hucht (1992) have categorized dusty WC’s as either “variable” or “persistent” dust-producers, based on the variability of IR flux. WR 140 and other variable sources consist of eccentric systems with $\gtrsim 10$ year orbits catalyzing dust formation only near periastron (Moffat et al. 1987; Williams et al. 1987b, 1990), while WR 104 and WR 98a have more circular orbits (possibly circularized at an earlier epoch; Monnier et al. 1999) with periods ~ 1 year, allowing continuous (“persistent”) dust production. An important unanswered question is whether all dusty WR sources lie somewhere along a continuum of binary orbits (Williams & van der Hucht 1992), or whether some of them could be single stars (Zubko 1998).

Another potential observational signature of binaries in dusty WR systems is non-thermal emission from colliding winds. However, one must first establish that non-thermal radio emission from a WR star requires a massive companion (van der Hucht et al. 1992). Recently, Dougherty & Williams (2000) re-examined just this question, and they found that known WR binaries with periods longer than 1 year do consistently show evidence for non-thermal radio emission, supporting the theory that colliding winds are responsible (Eichler & Usov 1993; Jardine et al. 1996). Further, Dougherty & Williams (2000) show that most binaries with periods less than 1 year have radio spectra similar to that expected for pure thermal wind sources (spectral index $\alpha^T \sim 0.65$), the intrinsic non-thermal emission presumably having been mostly absorbed by the ionized wind.

Having periods (~ 1 year) lying between the short and long period systems studied previously, it is unclear whether pinwheel nebulae should have detectable non-thermal radio emission. We have observed the confirmed pinwheel nebulae around WR 104 and WR 98a and the enigmatic candidate pinwheel WR 112 with the Very Large Array (VLA) of the National Radio Astronomy Observatory⁴ in order to characterize their radio properties. The goals of this study were to confirm

⁴The National Radio Astronomy Observatory is a facility of the National Science Foundation operated under cooperative agreement by Associated Universities, Inc.

the colliding wind origin of the pinwheel nebulae by definitive detection of non-thermal radio emission, to determine if there exists a distinctive radio signature that can be used as a diagnostic for binarity in systems whose infrared structure is too small or too dim to resolve (Monnier et al. 2001a), and to elucidate the true nature of the WR 112 system whose IR and radio properties have been difficult to understand (Ragland & Richichi 1999; Monnier et al. 2001b).

2. Observations and Results

We have used the Very Large Array (VLA) to measure the broadband spectra of three dust-enshrouded Wolf-Rayet systems, WR 104, WR 98a, and WR 112, at 1.43, 4.86, 8.46, 14.9, & 22.5 GHz. Before beginning our study, we cross-referenced the persistent and variable WR dust emitters from Williams & van der Hucht (1992) (which includes our target sample) with the southern hemisphere sample of Leitherer et al. (1997) and Chapman et al. (1999). Of the 12 sources in common, only two have been detected in the radio (WR 65 and WR 112). In order to have good chance to detect our program sources at most of the target wavelengths, our program was designed to improve upon the sensitivity limits of these previous surveys by factors of 3 to 10, with a goal of $\lesssim 100 \mu\text{Jy}$ ⁵ point-source sensitivity. The data reported here were collected during two separate observing runs, in 1999 September and 2000 February, when the VLA was in AnB and BnC configurations respectively; 3C286 was used for primary amplitude calibration. Poor observing conditions during the September epoch required some observations to be repeated in February. A preliminary report of our results appeared in Monnier et al. (2001a).

Since we were observing at five frequency bands, a number of secondary phase calibrators were used, and a complete journal of our calibrator observations appears in Table 1, including the adopted VLA calibrator positions and our new flux density measurements. In general we followed the guidelines of the VLA calibrator manual for amplitude calibration; however for WR 104 and WR 98a, we used the compact component of Sgr A* as a high-frequency calibrator by considering only (u,v) components beyond 50 k λ (100 k λ) at 8.46 & 14.9 GHz (22.5 GHz). Our 8.46 GHz flux estimates for Sgr A* are similar to contemporaneous measurements by G. C. Bower (personal communication, 2000), but our fluxes at higher frequencies are $\sim 15\%$ higher. This discrepancy may be due to slightly different cutoffs in (u,v) coverage employed during calibration or variability of Sgr A* itself (Zhao et al. 2001), but is also nearly consistent with the expected level of systematic errors in the amplitude calibration; our final conclusions do not hinge upon this possible source of miscalibration.

Table 2 contains the calibrated fluxes and source positions for the target sample, including the first radio detections of WR 104 and WR 98a. The resolution of the VLA in A-array is sufficient to resolve the thermal emission from some WR stars (e.g., Contreras & Rodríguez 1999), and the data

⁵1 Jy = 10^{-26} W m⁻² Hz⁻¹

Table 1: Journal of calibrator observations

Source	Position (J2000)		Date (U.T.)	Measured Flux Density ^{a,b} (Jy) at					Target Calibrated
	RA	Dec		1.43 GHz	4.86 GHz	8.46 GHz	14.9 GHz	22.5 GHz	
1733-130	17 33 02.7058	-13 04 49.548	1999 Sep 28	...	4.416	...	3.765	3.693	WR 112
			1999 Sep 29	3.833	...	
			2000 Feb 15	3.732	3.312	
Sgr A* ^c	17 45 40.0409	-29 00 28.118	1999 Sep 27	0.690	0.967	1.062	WR 104, WR 98a
			1999 Sep 28	0.744	0.869	1.014	
			2000 Feb 24	0.962	0.928	...	
			2000 Feb 25	1.003	
1751-253	17 51 51.2628	-25 24 00.063	1999 Sep 28	1.236	WR 104, WR 98
			1999 Sep 29	1.244	
			2000 Feb 15	1.229	
1820-254	18 20 57.8487	-25 28 12.584	1999 Sep 28	...	1.094	WR 98a
1832-105 ^d	18 32 20.8360	-10 35 11.200	1999 Sep 27	1.328	WR 112
			1999 Sep 28	...	1.174	
			2000 Feb 15	...	1.321	1.359	

^aFlux density scale was defined by the adopted strength of 3C286 using NRAO values of 14.75, 7.486, 5.181, 3.428, and 2.498 Jy at 1.43, 4.86, 8.46, 14.9, & 22.5 GHz respectively.

^bStatistical uncertainties were $\lesssim 1\%$. From the apparent scatter, we estimate systematic calibration uncertainties were generally better than 5%, but occasionally as bad as 10%.

^cSgr A* J2000 positions taken from Reid et al. (1999) measured on 1996.25 not correcting for apparent proper motion; this should be accurate to ~ 20 mas for the epoch of measurements reported here.

^dPositional accuracy < 150 mas. All others here have < 10 mas error.

were inspected for evidence of structure. Gaussian fits to the deconvolved images did not reveal any significant deviations from point sources.

We note that the 8.46 GHz measurement of WR 112 in 1999 September was corrupted by poor atmospheric phase stability, and the bispectrum was vector-averaged in order to extract an estimate of the point-source flux (for further discussion, see Cornwell 1987). This method is accurate only if no other sources are present in the field and if the target is unresolved, and the validity of these assumptions was checked using subsequent observations in 2000 February.

New positions and the associated uncertainties of the Wolf-Rayet stars were estimated by taking the mean and standard deviation of the right ascension and declination values found in Table 2, excluding data with unusually large errors (due to low elevation observations or calibrators with a poorly known positions). Our reported uncertainties are conservative, being based on the dispersion of the measurements rather than the uncertainty in the mean, since we lack sufficient independent observations to properly average over observing conditions. Table 3 contains these results along with the previously determined positions. The positions for WR 104 and WR 98a are significantly improved by this work, since the previous coordinates were based on optical and infrared observations, suffering from $\gtrsim 1''$ errors.

3. Modeling

3.1. Methodology

The radio data for each source were fit with a composite spectral model, consisting of a thermal wind source (F_ν^T) with non-thermal emission (F_ν^{NT}) absorbed by a variable amount of free-free opacity (τ_ν) from the overlying ionized wind. We note that F_ν^T is directly related to the total optical depth of the wind, but that in this model τ_ν represents only the optical depth along the line-of-sight to the non-thermal emission region F_ν^{NT} , which clearly must be less than or equal to the total opacity of the wind. This basic model has been used recently by several workers (Chapman et al. 1999; Skinner et al. 1999), and can be expressed in the following form (following Chapman):

$$F_\nu = F_{\nu,4.8 \text{ GHz}}^T \left(\frac{\nu}{4.8 \text{ GHz}} \right)^{\alpha^T} + F_{\nu,4.8 \text{ GHz}}^{NT} \left(\frac{\nu}{4.8 \text{ GHz}} \right)^{\alpha^{NT}} e^{-\tau_\nu} \quad (1)$$

where $F_{\nu,4.8 \text{ GHz}}$ refers to the flux density at 4.8 GHz.

For low signal-to-noise ratio (SNR) data of the weak sources (WR 104 and WR 98a), the free parameters of this model cannot all be independently well-constrained. Fortunately, the spectral indices for thermal and non-thermal emission have been measured for other Wolf-Rayet systems. We fix the spectral index of thermal emission (α^T) to be 0.65, which is representative of the range observed and predicted by theory (Leitherer & Robert 1991; Williams et al. 1990; Panagia & Felli 1975; Wright & Barlow 1975; Olon 1975). We also fix the spectral index of the non-thermal (α^{NT}) emission to -0.7, based on the range of values (-0.5 to -1.0) observed around other colliding wind sources (Skinner et al. 1999; Chapman et al. 1999; Dougherty et al. 1996; Setia Gunawan et al. 2000, 2001). The value of -0.5 can be physically motivated by considering Fermi acceleration of energetic electrons in the colliding wind shocks (Bell 1978) and subsequent synchrotron emission (for more detailed discussion, see Eichler & Usov 1993). Lastly, we fix the free-free opacity law to be $\tau_\nu = \tau_{4.8 \text{ GHz}} \left(\frac{\nu}{4.8 \text{ GHz}} \right)^{-2.1}$, which is appropriate for an electron temperature of $\sim 10^4$ K (see Eq. 3-57 in Spitzer 1978).

Table 4 contains the modeling results for our target stars, including 5% amplitude calibration errors (only important for WR 112). Because of the low SNR for WR 104 and WR 98a, the best-fitting parameters are not very meaningful, so we also report the full range of parameters values consistent with the data (i.e., the parameter range satisfying the condition that the reduced $\chi^2 < 1$).

3.2. WR 104

Figure 1 contains the modeling results for WR 104. A pure thermal model ($\alpha^T = 0.65$) is not a good fit (reduced $\chi^2 = 3.5$); there must be some non-thermal emission. This result is robust to the potential miscalibration at high frequencies using Sgr A* (discussed in §2), since potential

overestimate of the calibrator flux density would cause our estimate of the spectral index to be too high (i.e., more similar to thermal emission).

The maximum possible thermal emission component that can be supported by these new data is 0.36 mJy at 4.8 GHz. Interestingly, the data are consistent with *no* detectable thermal emission for models with large free-free optical depth. Unfortunately, the optical depth is not very well-constrained for WR 104 because the spectrum lacks reliable low-frequency detections. Quantitatively, the optical depth to the non-thermal emitting region at 4.8 GHz can range between 0.18 and 3.85 (best fitting value of 2.47) and still be consistent with the data. The resulting spectra from these scenarios, along with the best fitting spectrum, are included in Figure 1.

We note that WR 104 was searched for radio emission by Leitherer et al. (1997) and Chapman et al. (1999) who reported 3- σ upper limits of 1.59, 0.99, 2.01, & 0.39 mJy at 1.38, 2.38, 4.8, and 8.64 GHz respectively. Except for the 8.64 GHz observations, these results are consistent with the weak detections reported here.

3.3. WR 98a

Figure 2 contains the modeling results for WR 98a. WR 98a and WR 104 have qualitatively similar spectra, although a weak 4.86 GHz detection of WR 98a allows composite spectra models to be better constrained.

As for WR 104, a pure thermal model ($\alpha^T = 0.65$) is not consistent with these data (reduced $\chi^2=2.8$), and the maximum thermal emission at 4.8 GHz supported by the data is 0.24 mJy. The data are consistent with *no* detectable thermal emission for large free-free optical depths to the non-thermal emission region. These data constrain the optical depth to the non-thermal emitting region (at 4.8 GHz) to lie between 0.38 and 2.43 (best fit at 1.40), based largely on the 4.86 GHz detection.

3.4. WR 112

WR 112 was definitively detected by both Leitherer et al. (1997) and Chapman et al. (1999), and marked variability was observed between 1995 and 1997, probably caused by varying non-thermal radio emission. Our observations support this interpretation and reveal that WR 112 was in a radio-bright state between 1999 September and 2000 February. However at these recent epochs, we do not see evidence for the sharp drop (more than factor of 3) in flux density between 2.38 & 1.38 GHz reported by Chapman et al. (1999).

Figure 3 contains our modeling results for WR 112. At high frequencies, WR 112 shows a flat spectrum similar to WR 104 and WR 98a. However, there appears to be significantly less wind optical depth to the non-thermal emitting region ($\tau_{4.8\text{ GHz}} = 0.10$) here than for WR 104 and WR 98a.

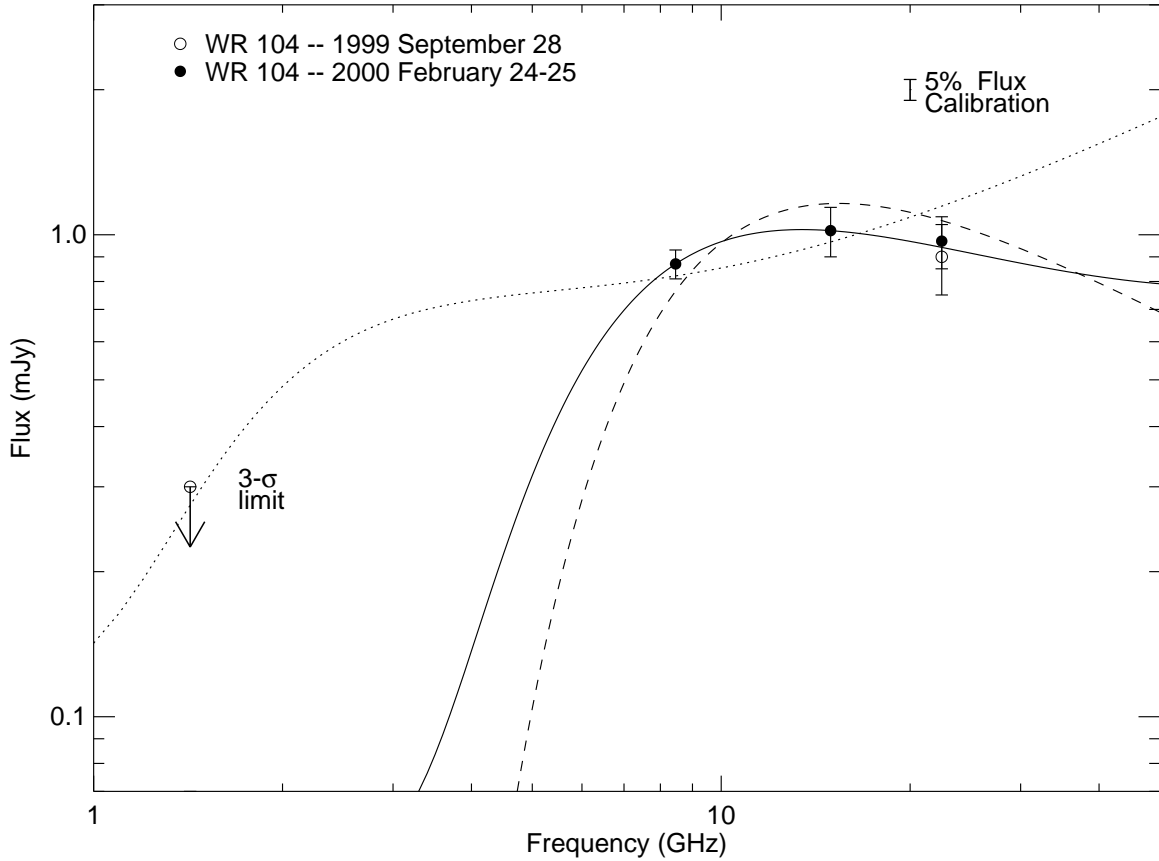


Fig. 1.— Broadband spectra of WR 104 with model fits. The best fitting model (reduced $\chi^2=0.024$) appears as a solid line while two other models also consistent with the data (reduced $\chi^2=1$) appear as a dotted line (tuned for maximum thermal emission, minimum non-thermal emission, minimum free-free absorption) and a dashed line (tuned for zero thermal emission, maximum non-thermal emission, maximum free-free absorption). See Table 4 for the values of the model parameters.

This supports the hypothesis that WR 112 is a longer period system than WR 104 and WR 98a, already suspected based on IR and radio variability considerations. There is some evidence for a decrease in the low-frequency flux density between 1999 September and 2000 February, corresponding to a $\sim 10\%$ decrease in the non-thermal emission component. We note that subsequent and on-going monitoring of WR 112 by our group confirms the trend of decreasing non-thermal emission with time, and full analysis of these variations will be considered in a future paper.

The high SNR data from 2000 February cannot be fitted by our simple model within the expected uncertainties (minimum reduced $\chi^2=1.75$), where the 5% amplitude calibration error generally dominates over the statistical measurement error. If we allow the spectral indices of the non-thermal and thermal components to deviate from their fixed values, the fit improves but is

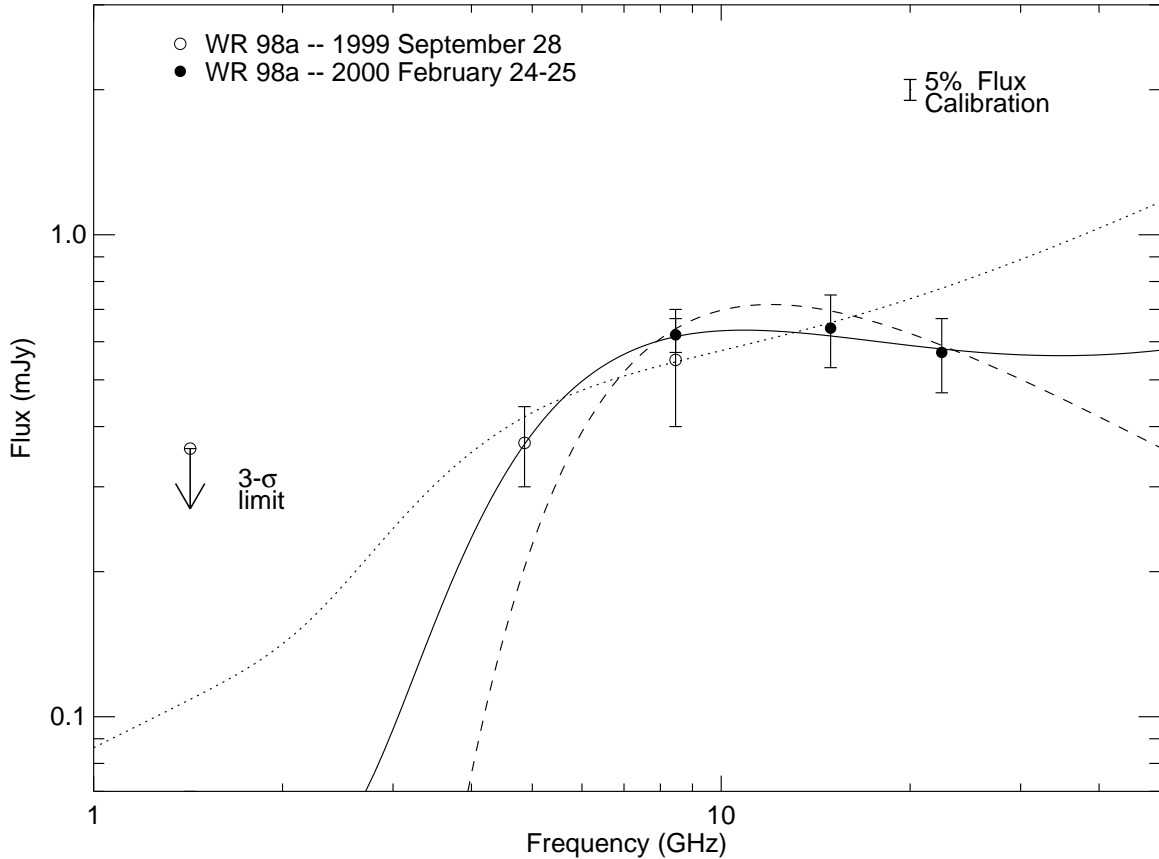


Fig. 2.— Broadband spectra of WR 98a with model fits. The best fitting model (reduced $\chi^2=0.040$) appears as a solid line while two other models also consistent with the data (reduced $\chi^2=1$) appear as a dotted line (tune for maximum thermal emission, minimum non-thermal emission) and a dashed line (adjusted for zero thermal emission, maximum non-thermal emission, maximum free-free absorption). See Table 4 for the values of the model parameters.

still not satisfactory. Specifically, if we insist that α^T lie between 0.6 and 0.7 and that α^{NT} stay between -0.5 and -1.0, the best fit model has a reduced $\chi^2=1.20$ (for $\alpha^T=.6$ and $\alpha^{NT}=-0.5$).

Skinner et al. (1999) (see also Setia Gunawan et al. 2001) fit the radio spectrum of long-period, colliding-wind binary WR 147 over a similar frequency range and found that an absorbed monoenergetic synchrotron spectrum fit the data better than the absorbed power-law model considered here. This better fit was largely due to a steep high-frequency cutoff observed in the non-thermal spectrum around 22 GHz which is more naturally accommodated by the synchrotron spectrum. A high-frequency cutoff is intimated in our WR 112 data but is uncertain due to difficulty in estimating the strength of the thermal emission. Skinner et al. (1999) were able to more reliably estimate the thermal emission component using 43 GHz observations and the fact that the thermal

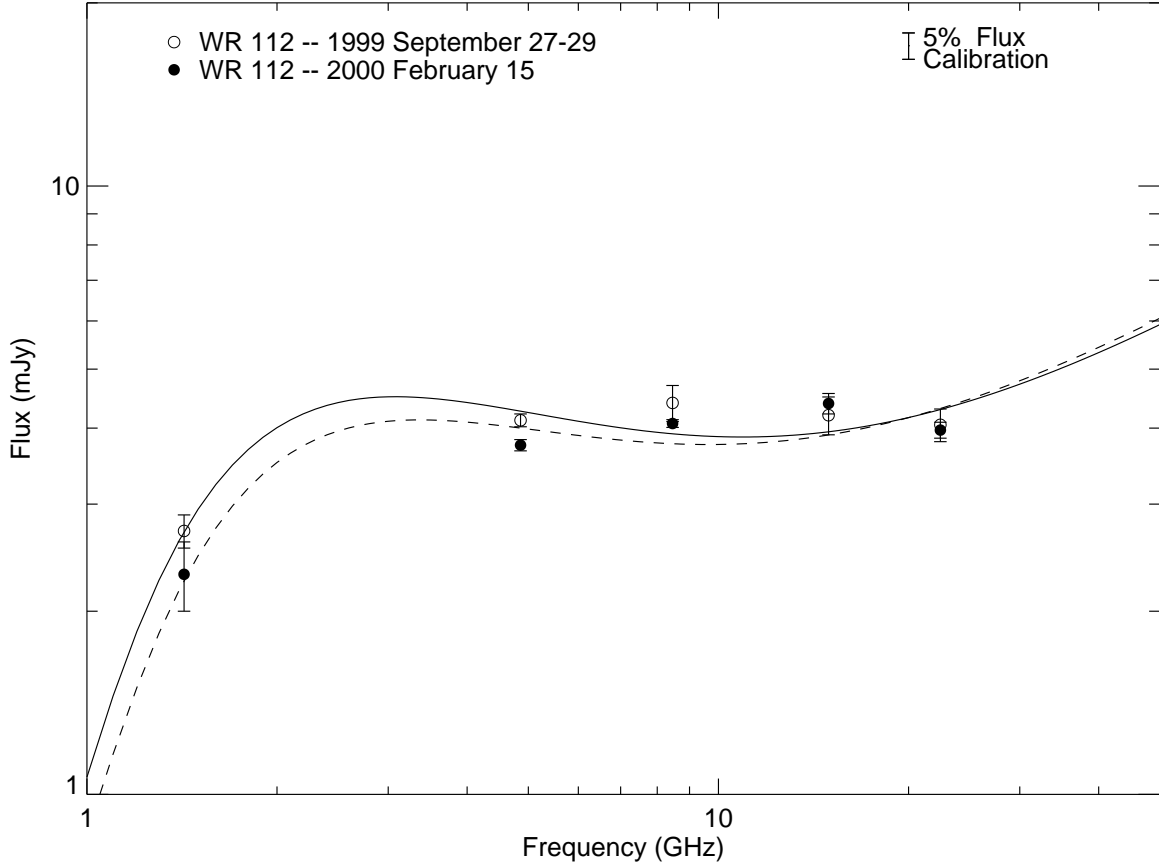


Fig. 3.— Broadband spectra of WR 112 with model fits for two epochs. The best-fitting model for September 1999 (reduced $\chi^2=0.63$) appears as a solid line while the best-fitting model for February 2000 (reduced $\chi^2=1.75$) appears as a dashed line. See Table 4 for the values of the model parameters.

and non-thermal components were spatially resolved from each other at both 15 GHz and 22 GHz.

4. Discussion

4.1. Thermal emission and mass-loss rates

The thermal emission from Wolf-Rayet stars is understood to arise from free-free emission in an expanding, ionized wind (Wright & Barlow 1975; Panagia & Felli 1975; Olon 1975). Following Wright & Barlow (1975), the observed flux density can be related to stellar and wind parameters

as follows:

$$F_\nu^T = 2.32 \times 10^4 \left(\frac{\dot{M}Z}{v_\infty \mu} \right)^{\frac{4}{3}} \left(\frac{\gamma g_\nu \nu}{d^3} \right)^{\frac{2}{3}} \quad (2)$$

where F_ν^T is the observed flux density in mJy, \dot{M} is the mass-loss rate in $M_\odot \text{ yr}^{-1}$, Z is the mean ionic charge, v_∞ is the wind velocity in km s^{-1} , μ is the mean molecular weight, γ is the mean number of electrons per ion, g_ν is the free-free Gaunt factor, ν is the observing frequency in Hz, and d is the distance in kpc.

Leitherer et al. (1997) discuss the best values to use for late-WC stars, and we have followed these authors in adopting $Z = 1.1$, $\gamma = 1.1$, $\mu = 4.7$, and $g_{4.8 \text{ GHz}} = 5.03$ in the calculations that follow. Table 5 contains the estimated distances and wind velocities of our targets derived from the literature, and fluxes from thermal emission at 4.8 GHz (from Table 4) based on the spectral decompositions of §3. With these data, equation (2) can be inverted to solve for the mass-loss rate, and these results are also contained in Table 5, corresponding to both the best-fitting values for the thermal emission component and the maximum allowed value. Also included in this table is an estimate of the major axis of the binary system based on the period and assumption of 15 M_\odot components.

The estimated mass-loss rates span 0.5 to $2.8 \times 10^{-5} M_\odot \text{ yr}^{-1}$, similar to results from previous studies of late-WC WR stars. (e.g., Nugis et al. 1998; Leitherer et al. 1997; Abbott et al. 1986). Because of the presence of non-thermal emission in all our sources, our determinations of mass-loss rate are very uncertain and we have neglected secondary effects such as clumping corrections (Moffat & Robert 1994; Morris et al. 2000). Interestingly, WR 112 seems to show a markedly higher ($2.5\times$) mass-loss rate than observed in 1995 (Leitherer et al. 1997) – that is, the high frequency radio emission (most likely dominated by thermal emission) was significantly higher in the more recent epochs. Although the orbital properties of the WR 112 binary are unknown, it is not expected that the thermal emission, which is dominated by free-free emission in the Wolf-Rayet wind, should be a strong function of the binary separation or other parameter. Higher frequency observations at multiple epochs can better isolate the thermal emission from non-thermal emission, critical for accurately estimating the mass-loss rates for individual colliding wind sources.

4.2. Non-thermal emission

As previously discussed in §3.4, the physical mechanism producing the non-thermal radio emission is not well known, and predictions from many models can be compared to the observed spectra (e.g., Skinner et al. 1999; Setia Gunawan et al. 2000, 2001). Despite these uncertainties, one component that all non-thermal emission models contain is free-free absorption by the overlying ionized wind. The free-free optical depth to the non-thermal emission implied by power-law models (as considered here) is generally larger than that obtained by fitting to alternative model spectra whose non-thermal source contain an intrinsic low-frequency turnover. Hence we can interpret the

optical depth parameters derived in the last section to be reasonable upper limits. We can therefore estimate a lower limit on wind depth where the emission arises, assuming only that the intrinsic non-thermal spectrum has low-frequency behavior flatter than the -0.7 spectral index used here for fitting (this includes the absorbed monoenergetic synchrotron spectrum preferred by Skinner *et al.* 1999).

In order to calculate the optical depth of the overlying wind for variously sized non-thermal emitting regions, we must first discuss how a binary system alters the wind density around the WR star. Let us consider a colliding wind system viewed nearly face-on, as is appropriate for the pinwheel nebulae WR 104 and WR 98a. The non-thermal radio emission originates at the interface of the colliding winds, which has a nearly conical geometry outside the interaction region (see Figure 4) with an opening angle, θ , dependent on the relative WR and O-star wind momenta. For wind momenta ratio between 0.01 and 0.1 (expected for these systems) the opening angle θ lies between 50° and 90° (Eichler & Usov 1993), consistent with the geometrical thickness of the dust plume seen around WR 104. In order to estimate the minimum intrinsic size of the non-thermal emission, we must calculate the impact parameter, ξ , which would intersect this cone with $\tau_{4.8 \text{ GHz}} \sim 1$. Because the integrated line-of-sight optical depth of the wind falls off steeply, $\tau \propto \xi^{-3}$ (Wright & Barlow 1975; Panagia & Felli 1975), this estimate is relatively insensitive to wind parameters. See Figure 4 for a sketch of the wind and orbital geometry.

For a generic late-WC wind with $\dot{M} = 1 \times 10^{-5} M_\odot \text{ yr}^{-1}$ and wind speed of 1000 km s^{-1} , the $\tau_{4.8 \text{ GHz}} \sim 1$ condition is reached for $\xi \sim 18, 15, 13 \text{ AU}$ for opening angles $\theta \sim 0^\circ, 60^\circ, 90^\circ$ respectively. For larger opening angles, the non-thermal emission extends more toward the observer and is visible at smaller impact parameters. Hence to be observed at all, the intrinsic non-thermal emission region must extend along the interface cone to this distance ξ . This size is significantly larger than the estimated non-thermal emission region size estimated by Eichler & Usov (1993), which was largely based on what scale the wind collision can efficiently put energy into the shocks (1 to 3 AU for our target stars).

It has been pointed out by previous investigators that the estimated optical depth to the shock collision zone is so large that all non-thermal radio emission should be completely obscured for periods $\lesssim 2 \text{ yr}$ (Dougherty & Williams 2000; Chapman *et al.* 1999; White & Becker 1995; Williams *et al.* 1990, 1994). Most recently, Dougherty & Williams (2000) discuss a number of explanations for why nonthermal emission is visible for WR 11 ($\gamma^2 \text{ Vel}$, period 78.53 days). At radio wavelengths, one can see deeper into the wind if it is clumpy (e.g, Nugis *et al.* 1998) or non-spherical (Williams *et al.* 1997). In addition for nearly edge-on systems, lines-of-sight can pass through the relatively less-dense O-star wind during some parts of the orbit, causing the observed radio spectrum to vary.

Since the WR 104 and WR 98a binaries are viewed within $\sim 35^\circ$ from face-on (Monnier *et al.* 1999), we can eliminate possible explanations invoking novel observing geometries, such as viewing the collision zone through the O-star wind. Further, the wind would need to be very clumpy and/or non-spherical to allow emission at $\xi \sim 1\text{-}3 \text{ AU}$ to be visible, considering that $\tau_\nu \propto \xi^{-3}$; the 4.8 GHz

optical depth in the smooth wind to the collision zone is ~ 50 for typical late-WC stars. Such radical departures from smooth flow would likely be seen as significant changes to the thermal emission, which arises from the same ionized wind material.

Here we develop another possibility, that the non-thermal emission region may be intrinsically larger than expected (also suggested in part by Dougherty & Williams 2000). The plasma could continue to radiate beyond the initial collision region for at least the synchrotron cooling timescale. In order for the plasma to travel out of the collision region and reach the $\tau_{4.8 \text{ GHz}} \sim 1$ surface, this time would need to be $\gtrsim 10$ days, a reasonable time span considering the analysis of Eichler & Usov (1993, see §3), assuming magnetic fields of a few Gauss. The size and strength of the radio emission “tail” also depends greatly on the magnetic field geometry; for uniform magnetic fields the energetic electrons can escape to greater distances from the collision region than for non-uniform magnetic fields, and could produce observable radio emission (Usov 2001, private communication); thus these observations might be revealing important new information regarding the magnetic fields of WR+OB binaries. Interestingly, Corcoran et al. (1996) found evidence that the X-ray emitting region of the colliding wind system V444 Cyg (WR 139), presumed to trace hot shocked gas, was also unexpectedly large ($10\times$ the binary separation). Lastly, it might be possible that even compact non-thermal radio emission may appear larger due to electron scattering in the dense ionized wind.

We have calculated the minimum impact parameter ξ for each of our target stars based on the (best-fit) estimated mass-loss rates, the orbital and wind parameters, the upper-limit of $\tau_{4.8 \text{ GHz}}$ derived from our spectral fits, and a cone angle of 60° . From this minimum ξ , we can estimate the minimum extent of the non-thermal emission, R^{NT} , by subtracting the binary separation from the minimum ξ (since the dense WR wind is centered on the WR star while the collision region occurs close to the OB-star). These values have been placed in Table 5 and should be taken as lower limits to the intrinsic size of the non-thermal emission region; the non-thermal emission region could be much larger since we are adopting conservative upper-limits for the optical depth.

This model can be tested by high-resolution imaging of the non-thermal radiation, but VLBA observations of WR 104 and WR 98a are currently not practical due to their weak flux. While WR 112 is bright enough to detect (in its radio-bright state), the closest phase reference calibrator is $\sim 5^\circ$ away. Initial attempts to image the non-thermal radio emission (by our group) have failed either because the source was over-resolved or due to spatial incoherence effects attributed to low elevation and the large angular distance between the WR 112 and the phase reference. VLBA observations of closer colliding wind sources, such as WR 140 near periastron or WR 11, should be able to resolve these structures and determine precisely the physical geometry of the non-thermal emitting regions.

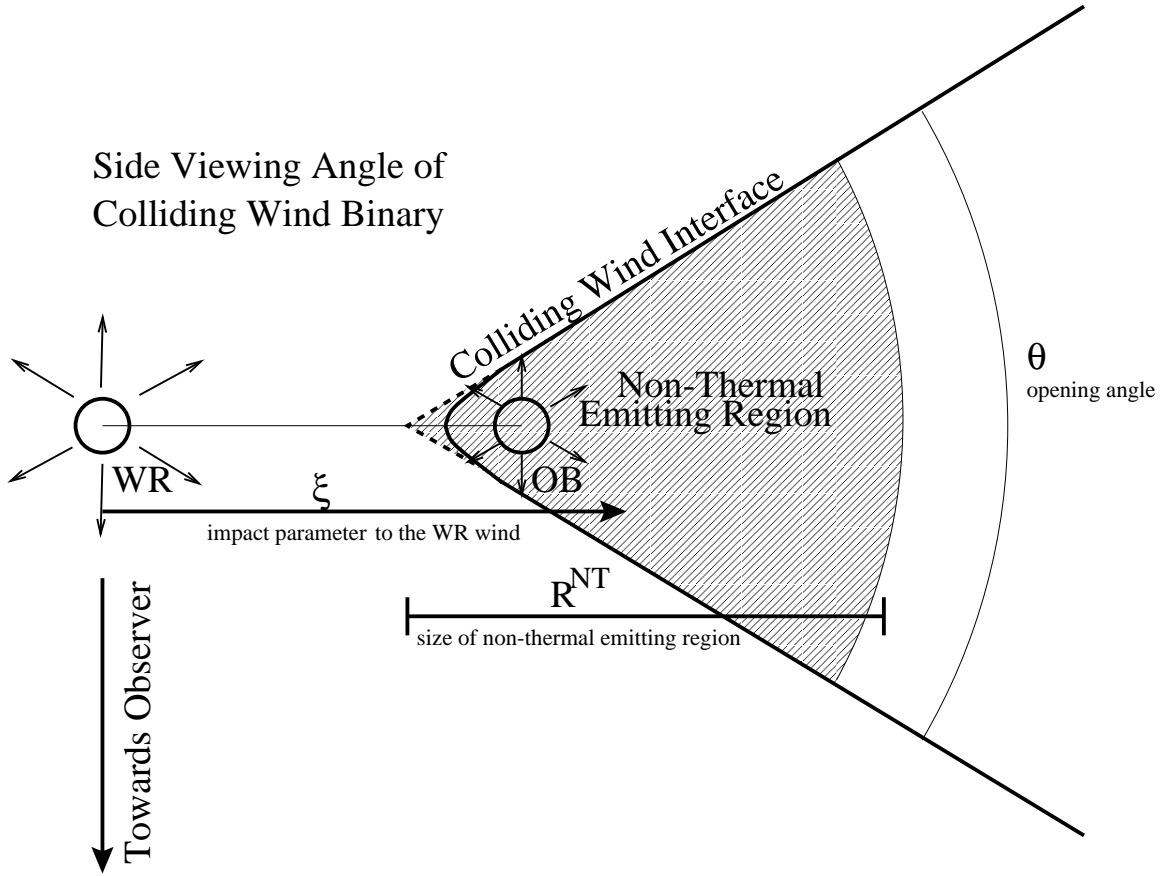


Fig. 4.— Schematic of colliding wind geometry for WR+OB binaries (not to scale). The intrinsic size of the non-thermal emitting region can be estimated from the observed lower limits on the wind optical depth. See Table 5 for the values of the model parameters.

4.3. Effects of dust on the radio emission

If the dust formed at the colliding wind interface is optically thick to UV-photons, a significant fraction of the circumstellar gas will be shielded from the ionizing flux of the central sources. Figure 5 shows an idealized model of colliding wind interface geometry for WR 104 (for opening angle $\theta = 90^\circ$). The radius of the WR 104 radio photosphere is ~ 15 AU at 4.8 GHz ($\propto \nu^{-0.66}$, Wright & Barlow 1975), which is similar to the length scale of the spiral wind interface in Figure 5. Hence, dust in the interface region can absorb the UV flux and shadow a significant volume of the wind (especially in the mid-plane). Initial calculations indicate that the thermal emission will be smaller by $\sim 30\%$ for the same mass-loss rate, and the spectral slope might be slightly larger than the canonical $\alpha^T \sim 0.65$. We note that these effects may even be important for spherical distributions of grains, since the inner radius of the dust shell in such models is also ~ 25 AU (Zubko 1998) and could change the ionization fraction in the outer envelope from standardly-used

values.

The brightness of the non-thermal radio emission could also be affected. For binary systems viewed nearly edge-on, the dust shadow would also significantly reduce the line-of-sight opacity to the collision zone (since the gas will not be ionized in the shadow) at certain orbital phases than currently expected. More work is needed to quantitatively understand these effects, and will need to include a detailed treatment of the dust opacity as well as recombination time scale for “shadowed”-gas.

Such effects could be detected with high resolution images of the thermal emission region, since the shadowing would cause the emission to be very asymmetrical. By observing at mm-wave wavelengths, it would be possible to probe deeper layers on the wind, revealing the structure of the wind-wind interface on ~ 10 AU scales (e.g., using MERLIN, ALMA). In addition, signs of shadowing might also be seen on larger scales in nebular emission lines or as linear polarization at visible wavelengths.

4.4. Time-variability

Unfortunately, all our observations of individual sources at different frequencies were not taken at the same epoch, which is potentially troubling since WR 104 and WR 98a are known to have binary periods of 243.5 and 565 days respectively (Monnier et al. 1999). Fortunately, there is some wavelength overlap between the epochs for both sources and these flux measurements are consistent to within errors. This is not surprising for WR 104 since analysis of the spiral morphology indicates a nearly face-on viewing angle ($11 \pm 7^\circ$, Monnier 1999). There is some IR flux variation observed for WR 98a (Williams et al. 1995), either due to optical depth effects (viewing angle is ~ 35 degrees for WR 98a) or orbital eccentricity, but we do not detect a similar radio variation in our limited dataset. In both cases, the colliding wind interface should not cross our line-of-sight and hence we do not expect large variations of the kind seen in other systems, such as WR 140 (White & Becker 1995).

WR 112 showed evidence for slight variation between 1999 September and 2000 February at low frequencies. We are monitoring this source with the VLA in order to understand the large variation originally observed by Leitherer et al. (1997) and Chapman et al. (1999). This variation can be either due to changes in line-of-sight opacity or intrinsic radio emission, caused by either a large inclination angle or binary separation (or both). Coordinated infrared imaging and broadband radio spectra will go a long way towards supporting the creation of a self-consistent model, and clarifying the likely cause(s) of the observed variability.

5. Conclusions

We detected non-thermal radio emission from both known pinwheel nebulae (WR 104 and WR 98a) and the suspected binary system WR 112. Pure thermal emission from a spherically-symmetric ionized wind was not consistent with the spectra from any of the sources, and some non-thermal emission was always required to explain the observations. Simple composite spectral models were fit to the broadband measurements, allowing emission strengths of the thermal and non-thermal components to be estimated along with the line-of-sight opacity towards the non-thermal emission region. From the inferred thermal emission strengths and known wind properties, we estimated the mass-loss rates and found them to be similar to those for other late-WC WR stars, validating the basic spectral decomposition employed here.

Using these results, the upper bound line-of-sight opacities to the non-thermal emission were inverted to estimate lower-limit sizes of the non-thermal emission regions, which were many times larger than expected from current theory (Eichler & Usov 1993). We suggest that synchrotron cooling times of a few weeks would allow the radio-emitting plasma to travel into an optically thin portion of the thermal WR wind and to be observed, or that uniform magnetic fields could allow energetic electrons to escape out of the radio “photosphere.”

We also discussed implications of dust obscuration on the radio properties of dusty WRs. If the dust in the outflow is optically thick to ultraviolet photons, a significant fraction of the wind will be shadowed from the major sources of ionization. This will affect mass-loss rates determined from high frequency radio observations for all binary (i.e. non-thermal) systems and could cause dramatic differences in the line-of-sight free-free opacity for binary systems viewed edge-on.

A lack of high frequency (e.g., 43 GHz) observations hampered our analysis since even 22 GHz observations were significantly contaminated by non-thermal radio emission, making the decomposition of spectra reliant on *a priori* estimates for the model spectral indices. For WR 112, high SNR measurements suggest that simple two-component power-law models commonly used are inadequate, hinting at a high frequency turnover to the non-thermal radio emission. We emphasize that further progress in this field will require multi-wavelength simultaneous observations from 1 to 43 GHz in order to untangle the contributions from the thermal and non-thermal components.

The hypothesis that colliding winds lie at the heart of all Wolf-Rayet dust shells has passed another observational test, detection of non-thermal radio emissions from WR 104, WR 98a, and WR 112. A sensitive radio survey ($\sigma \lesssim 0.1$ mJy) between 1 and 43 GHz of all known dusty Wolf-Rayets would put this hypothesis to a final challenge.

The authors would like to recognize useful discussions and comments from S. Dougherty and V. Usov. This research has made use of the SIMBAD database, operated at CDS, Strasbourg, France, and NASA’s Astrophysics Data System Abstract Service. JDM acknowledges support from a Center for Astrophysics Fellowship at the Harvard-Smithsonian Center for Astrophysics.

REFERENCES

- Abbott, D. C., Torres, A. V., Biegging, J. H., & Churchwell, E. 1986, *ApJ*, 303, 239
- Bell, A. R. 1978, *MNRAS*, 182, 147
- Chapman, J. M., Leitherer, C., Koribalski, B. ., Bouter, R., & Storey, M. 1999, *ApJ*, 518, 890
- Contreras, M. E. & Rodríguez, L. F. 1999, *ApJ*, 515, 762
- Corcoran, M. F., Stevens, I. R., Pollock, A. M. T., Swank, J. H., Shore, S. N., & Rawley, G. L. 1996, *ApJ*, 464, 434
- Cornwell, T. J. 1987, *A&A*, 180, 269
- Dougherty, S. M. & Williams, P. M. 2000, *MNRAS*, 319, 1005
- Dougherty, S. M., Williams, P. M., van der Hucht, K. A., Bode, M. F., & Davis, R. J. 1996, *MNRAS*, 280, 963
- Eichler, D. & Usov, V. 1993, *ApJ*, 402, 271
- Jardine, M., Allen, H. R., & Pollock, A. M. T. 1996, *A&A*, 314, 594
- Leitherer, C., Chapman, J. M., & Koribalski, B. 1997, *ApJ*, 481, 898
- Leitherer, C. & Robert, C. 1991, *ApJ*, 377, 629
- Moffat, A. F. J., Lamontagne, R., Williams, P. M., Horn, J., & Seggewiss, W. 1987, *ApJ*, 312, 807
- Moffat, A. F. J. & Robert, C. 1994, *ApJ*, 421, 310
- Monnier, J. D. 1999, PhD thesis, University of California at Berkeley
- Monnier, J. D., Greenhill, L. J., Tuthill, P. G., & Danchi, W. C. 2001a, in *ASP Conf. Ser.:* Interacting Winds from Massive Stars, in press
- Monnier, J. D., Tuthill, P. G., & Danchi, W. C. 1999, *ApJ*, 525, L97
- . 2001b, *ApJ*, in preparation
- Morris, P. W., van der Hucht, K. A., Crowther, P. A., Hillier, D. J., Dessart, L., Williams, P. M., & Willis, A. J. 2000, *A&A*, 353, 624
- Nugis, T., Crowther, P. A., & Willis, A. J. 1998, *A&A*, 333, 956
- Olson, F. M. 1975, *A&A*, 39, 217
- Panagia, N. & Felli, M. 1975, *A&A*, 39, 1

- Ragland, S. & Richichi, A. 1999, MNRAS, 302, L13
- Reid, M. J., Readhead, A. C. S., Vermeulen, R. C., & Treuhaft, R. N. 1999, ApJ, 524, 816
- Setia Gunawan, D. Y. A., de Bruyn, A. G., van der Hucht, K. A., & Williams, P. M. 2000, A&A, 356, 676
- . 2001, A&A, 368, 484
- Skinner, S. L., Itoh, M., Nagase, F., & Zhekov, S. A. 1999, ApJ, 524, 394
- Spitzer, L. 1978, Physical processes in the interstellar medium (New York Wiley-Interscience, 1978. 333 p.)
- Tuthill, P. G., Monnier, J. D., & Danchi, W. C. 1999, Nature, 398, 487
- Tuthill, P. G., Monnier, J. D., & Danchi, W. C. 2001, in ASP Conf. Ser.: Interacting Winds from Massive Stars, in press
- Usov, V. V. 1991, MNRAS, 252, 49
- van der Hucht, K. A. 2001, New Astronomy Review, 45, 135
- van der Hucht, K. A., Williams, P. M., Spoelstra, T. A. T., & de Bruyn, A. C. 1992, in ASP Conf. Ser. 22: Nonisotropic and Variable Outflows from Stars, 249
- White, R. L. & Becker, R. H. 1995, ApJ, 451, 352+
- Williams, M. & van der Hucht, K. A. 1992, in ASP Conf. Ser. 22: Nonisotropic and Variable Outflows from Stars, 269
- Williams, P. M., Cohen, M., van der Hucht, K. A., Bouchet, P., & Vacca, W. D. 1995, MNRAS, 275, 889+
- Williams, P. M., Dougherty, S. M., Davis, R. J., van der Hucht, K. A., Bode, M. F., & Setia Gunawan, D. Y. A. 1997, MNRAS, 289, 10
- Williams, P. M., van der Hucht, K. A., Pollock, A. M. T., Florkowski, D. R., van der Woerd, H., & Wamsteker, W. M. 1990, MNRAS, 243, 662
- Williams, P. M., van der Hucht, K. A., & Spoelstra, T. A. T. 1994, A&A, 291, 805
- Williams, P. M., van der Hucht, K. A., & The, P. S. 1987a, A&A, 182, 91
- Williams, P. M., van der Hucht, K. A., van der Woerd, H., Wamsteker, W. M., & Geballe, T. R. 1987b, in ASSL Vol. 136: Instabilities in Luminous Early Type Stars, 221–226
- Wright, A. E. & Barlow, M. J. 1975, MNRAS, 170, 41

Zhao, J., Bower, G. C., & Goss, W. M. 2001, *ApJ*, 547, L29

Zubko, V. G. 1998, *MNRAS*, 295, 109+

Table 2: Journal of Wolf-Rayet observations

Target Star	Date (U.T.)	Observing	Measured Flux ^{a,b,c} Density (mJy)	Position (J2000) ^d		Comments ^e
		Frequency Band (GHz)		RA	Dec	
WR 104	1999 Sep 28	L (1.425)	<0.30	-	-	
	2000 Feb 24	X (8.460)	0.87±0.06	18 02 04.128±0.006	-23 37 42.14±0.05	Unresolved
	2000 Feb 24	U (14.94)	1.02±0.12	18 02 04.110±0.005	-23 37 42.40±0.07	Unresolved
	1999 Sep 28	K (22.46)	0.90±0.15	18 02 04.127±0.001	-23 37 42.18±0.01	Unresolved
	2000 Feb 25	K (22.46)	0.97±0.12	18 02 04.126±0.005	-23 37 42.25±0.08	Unresolved
WR 98A	1999 Sep 28	L (1.425)	<0.36	-	-	
	1999 Sep 28	C (4.860)	0.37±0.07	17 41 13.044	-30 32 30.25	Weak Detection
	1999 Sep 28	X (8.460)	0.55±0.15	17 41 13.044±0.005	-30 32 30.35±0.10	Weak Detection
	2000 Feb 24	X (8.460)	0.62±0.05	17 41 13.057±0.006	-30 32 30.39±0.06	Unresolved
	2000 Feb 24	U (14.94)	0.64±0.11	17 41 13.047±0.008	-30 32 30.23±0.18	
	2000 Feb 25	K (22.46)	0.57±0.10	17 41 13.054±0.008	-30 32 30.38±0.10	
WR 112	1999 Sep 29	L (1.425)	2.71±0.17	18 16 33.484±0.002	-18 58 42.79±0.03	Unresolved
	2000 Feb 15	L (1.425)	2.3±0.30	18 16 33.484±0.006	-18 58 42.36±0.13	Unresolved
	1999 Sep 28	C (4.860)	4.12±0.10	18 16 33.488±0.030	-18 58 42.47±0.30	Unresolved ^f
	2000 Feb 15	C (4.860)	3.75±0.08	18 16 33.490±0.001	-18 58 42.33±0.02	Unresolved
	1999 Sep 27	X (8.460)	4.4±0.3	-	-	Bispectrum ^g
	2000 Feb 15	X (8.460)	4.07±0.06	18 16 33.4879±0.0003	-18 58 42.289±0.006	Unresolved
	1999 Sep 29	U (14.94)	4.2±0.3	18 16 33.490±0.001	-18 58 42.50±0.01	Unresolved
	2000 Feb 15	U (14.94)	4.39±0.17	18:16 33.4902±0.0004	-18 58 42.347±0.010	Unresolved
	1999 Sep 28	K (22.46)	4.05±0.25	18 16 33.4912±0.0001	-18 58 42.353±0.002	Unresolved
	2000 Feb 15	K (22.46)	3.97±0.12	18 16 33.4901±0.0003	-18 58 42.374±0.007	Unresolved

^aFlux density determined using AIPS tasks JMFIT and MAXFIT.

^bWhen not detected, we report 3- σ upper limits.

^cFlux uncertainties here include only measurement error, not systematic calibration uncertainties which are generally $\sim 5\%$.

^dPosition estimates and errors derived from fits to a single Gaussian.

^e“Unresolved”: Gaussian fit to image consistent with point source response (FWHM less than one-third of beam). Blank: too little flux density to adequately constrain a Gaussian fit; the flux density reported assumes the source is unresolved.

^fLow elevation observations ($\sim 13^\circ$) had poor phase calibration, resulting in degraded astrometry; self-calibration was possible to retain precise photometry.

^gPhase stability was too poor to successfully phase reference. However, the flux for WR 112 was estimated by vector-averaging the bispectrum. See §2 for more details.

Table 3: Radio positions of Wolf-Rayet stars

Source	New Radio Position ^a (J2000)		Previous Position ^b (J2000)	
	RA	Dec	RA	Dec
WR 104	18 02 04.123 ± 0.009	-23 37 42.24 ± 0.11	18 02 04.07	-23 37 41.2
WR 98a	17 41 13.051 ± 0.006	-30 32 30.34 ± 0.07	17 41 12.9	-30 32 29
WR 112 ^c	18 16 33.489 ± 0.003	-18 58 42.47 ± 0.19	18 16 33.49	-18 58 42.5

^aThis work.

^bFrom the VIIth Catalogue of Wolf-Rayet Stars by van der Hucht (2001). WR 104 and WR 98a positions were from optical observations while the position of WR 112 was derived from radio work.

Table 4: Results from two-component model fitting

Model Parameters	WR 104		WR 98a		WR 112			
					Sep 1999		Feb 2000	
$F_{\nu, 4.8 \text{ GHz}}^T$ (mJy)	0.072	[0 - 0.36] ^a	0.078	[0 - 0.24]	1.14	[0.97 - 1.32]	1.18	[–] ^b
α^T	0.65	[Fixed]	0.65	[Fixed]	0.65	[Fixed]	0.65	[Fixed]
$F_{\nu, 4.8 \text{ GHz}}^{NT}$ (mJy)	2.42	[0.78 - 3.70]	1.14	[0.33 - 1.96]	3.47	[3.01 - 3.94]	3.16	[–]
α^{NT}	-0.70	[Fixed]	-0.70	[Fixed]	-0.70	[Fixed]	-0.70	[Fixed]
$\tau_{4.8 \text{ GHz}}$	2.47	[0.18 - 3.85]	1.40	[0.38 - 2.43]	0.10	[0.088 - 0.11]	0.11	[–]
Reduced χ^2	0.024		0.040		0.63		1.75	

^aThe best fitting parameters appear in the table, while the range of acceptable values follow in brackets (as judged by a final reduced $\chi^2 < 1$).

^bThe best-fitting model had a reduced $\chi^2 > 1$.

Table 5: Derived parameters based on radio spectra

Source	Distance (kpc)	v_∞ (km s ⁻¹)	a^a (AU)	$F_{4.8 \text{ GHz}}^T$ (mJy)	Max $\tau_{4.8 \text{ GHz}}$	Refs	M (10 ⁻⁵ M _⊙ yr ⁻¹)	R ^{NTb} (AU)
WR 104 (WC9)	2.3	1220	2.4	0.072 (< 0.36) ^c	3.9	1,4	0.8 (< 2.8)	>5
WR 98a (WC8-9)	1.9	900	4.1	0.078 (< 0.24)	2.4	2,4	0.5 (< 1.1)	>4
WR 112 (WC9)	1.3	1100	6.1 ^d	1.16±0.17	0.11	3,4	2.5±0.3 ^e	~46 ^f

^aBinary separation based on the orbital period and the assumption that both components are 15 M_⊙.

^bTransverse distance from shock stagnation point to location corresponding to wind opacity $\tau_{4.8 \text{ GHz}}$; estimate of the intrinsic size of the non-thermal emission (see discussion in §4.2)

^cQuantities in parentheses represent upper limits based on fits to radio spectra.

^dPeriod of WR 112 binary is unknown, but estimated to be ~1000 days based on unpublished radio and IR data.

^eThis error bar only reflects errors in determining $F_{4.8 \text{ GHz}}^T$, and not the much larger uncertainties in the distance and wind velocity.

^fThis assumes line-of-sight does not traverse the OB-star wind, but only the WR wind.

References. — 1. Tuthill et al. (1999). 2. Monnier et al. (1999). 3. Nugis et al. (1998). 4. This work.

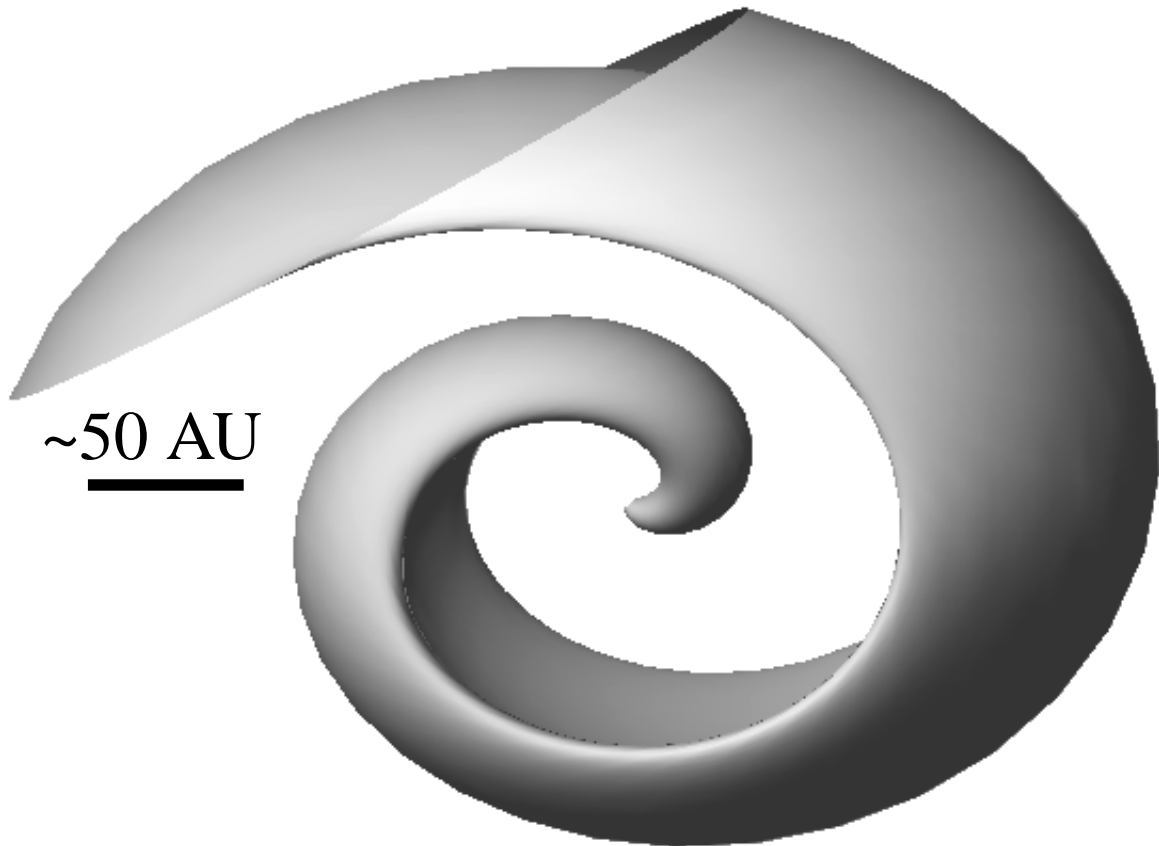


Fig. 5.— Three-dimensional representation of the colliding wind interface for WR 104. In this picture, the two stars are located in the very center separated by a few AU horizontally. As the stars orbit (clockwise), the shock cone wraps around into a thin, quasi-spherical sheet. The termination of this surface is defined for material which left the WR star at the same time. If the dust exists in a thin sheet at this interface, the optical depth could be sufficient to block stellar ultra-violet photons from ionizing the wind and thus reduce the observed free-free emission.